

Magnetic properties and promising cryogenic magneto-caloric performances of $Gd_{20}Ho_{20}Tm_{20}Cu_{20}Ni_{20}$ amorphous ribbons

Yikun Zhang(张义坤), Bingbing Wu(吴兵兵), Dan Guo(郭丹), Jiang Wang(王江), and Zhongming Ren(任忠鸣)
Citation: Chin. Phys. B, 2021, 30 (**1**): 017501. DOI: 10.1088/1674-1056/abc0d7
Journal homepage: http://cpb.iphy.ac.cn; http://iopscience.iop.org/cpb

What follows is a list of articles you may be interested in

Giant anisotropy of magnetic damping and significant in-plane uniaxial magnetic anisotropy in amorphous $Co_{40}Fe_{40}B_{20}$ films on GaAs(001)

Ji Wang(王佶), Hong-Qing Tu(涂宏庆), Jian Liang(梁健), Ya Zhai(翟亚), Ruo-Bai Liu(刘若柏), Yuan Yuan(袁源), Lin-Ao Huang(黄林傲), Tian-Yu Liu(刘天宇), Bo Liu(刘波), Hao Meng(孟皓), Biao You(游彪), Wei Zhang(张维), Yong-Bing Xu(徐永兵), Jun Du(杜军)
Chin. Phys. B, 2020, 29 (**10**): 107503. DOI: 10.1088/1674-1056/abad1d

Magnetic characterization of a thin $Co_2MnSi/L1_0$–MnGa synthetic antiferromagnetic bilayer prepared by MBE

Shan Li(黎姗), Jun Lu(鲁军), Si-Wei Mao(毛思玮), Da-Hai Wei(魏大海), Jian-Hua Zhao(赵建华)
Chin. Phys. B, 2020, 29 (**10**): 107501. DOI: 10.1088/1674-1056/ab99ac

A novel diluted magnetic semiconductor $(Ca,Na)(Zn,Mn)_2Sb_2$ with decoupled charge and spin dopings

Yilun Gu(顾轶伦), Haojie Zhang(张浩杰), Rufei Zhang(张茹菲), Licheng Fu(傅立承), Kai Wang(王恺), Guoxiang Zhi(智国翔), Shengli Guo(郭胜利), Fanlong Ning(宁凡龙)
Chin. Phys. B, 2020, 29 (**5**): 057507. DOI: 10.1088/1674-1056/ab892e

Microstructure and ferromagnetism ofheavily Mn doped SiGe thin flims

Huanming Wang(王焕明), Sen Sun(孙森), Jiayin Xu(徐家胤), Xiaowei Lv(吕晓伟), Yuan Wang(汪渊), Yong Peng(彭勇), Xi Zhang(张析), Gang Xiang(向钢)
Chin. Phys. B, 2020, 29 (**5**): 057504. DOI: 10.1088/1674-1056/ab8219

Effect of annealing temperature on coercivity of Nd-Fe-B magnets with TbFeAl doping by process of hot-pressing

Ze-Teng Shu(舒泽腾), Bo Zheng(郑波), Guang-Fei Ding(丁广飞), Shi-Cong Liao(廖是聪), Jing-Hui Di(邸敬慧), Shuai Guo(郭帅), Ren-Jie Chen(陈仁杰), A-Ru Yan(闫阿儒), Lei Shi(石磊)
Chin. Phys. B, 2020, 29 (**5**): 057501. DOI: 10.1088/1674-1056/ab7b57

Magnetic properties and promising cryogenic magneto-caloric performances of $Gd_{20}Ho_{20}Tm_{20}Cu_{20}Ni_{20}$ amorphous ribbons*

Yikun Zhang(张义坤)[1,2,3,†], Bingbing Wu(吴兵兵)[1,2,3], Dan Guo(郭丹)[1,2,3], Jiang Wang(王江)[1,2,3], and Zhongming Ren(任忠鸣)[1,2,3]

[1] *State Key Laboratory of Advanced Special Steels, Shanghai University, Shanghai* 200072, *China*
[2] *Shanghai Key Laboratory of Advanced Ferrometallurgy, Shanghai University, Shanghai* 200072, *China*
[3] *School of Materials Science and Engineering, Shanghai University, Shanghai* 200072, *China*

(Received 3 June 2020; revised manuscript received 3 October 2020; accepted manuscript online 14 October 2020)

The magnetic cooling utilizing magneto-caloric effect is recognized as promising energy efficiency and environmentally friendly technology. Here we report a systematical study on the microstructures, magnetic properties and cryogenic magneto-caloric performances of the $Gd_{20}Ho_{20}Tm_{20}Cu_{20}Ni_{20}$ amorphous ribbons. It is found that the ribbons reveal a second-order phase transition and are accompanied by a table-shaped magneto-caloric effect. The calculated magnetic-entropy-change maximum $|\Delta S_M|$, temperature averaged entropy change (i.e., TEC(10)), and refrigerant capacity reach 13.9 J/kg·K, 13.84 J/kg·K and 740 J/kg with magnetic field change of 0–7 T, respectively, indicating that the present $Gd_{20}Ho_{20}Tm_{20}Cu_{20}Ni_{20}$ amorphous ribbons are good candidates for magnetic cooling.

Keywords: microstructure, magneto-caloric effect (MCE), amorphous ribbons, magnetic properties

PACS: 75.30.Sg, 64.70.pe, 75.50.Kj **DOI:** 10.1088/1674-1056/abc0d7

Nowadays, the interest in research on magnetic solids with promising magneto-caloric performances has considerably grown due to the potential applications in the field for future magnetic cooling (MC).[1–4] Magneto-caloric effect (MCE) is a magneto-thermodynamic property of magnetic solids, which depends on the interaction between external field and magnetic sub-lattices. Generally, MCE is characterized by two important factors, i.e., magnetic entropy change ΔS_M and refrigerant capacity (RC), when the external field changes. Due to special characterizations of promising high-efficiency and environmental friendliness, the MCE-based cooling technology would be able to replace the presently available gas compression/expansion cooling technology.[1–4] The Ericsson cycles consisting of two isomagnetic fields and two isothermal processes have been recognized as the best choice for cryogenic MC. For the most ideal Ericsson MC cycles, the magneto-caloric materials should have constant ΔS_M in the whole cooling temperature range, i.e., a table-shaped MCE.[5,6] This performance can be indirectly identified with the help of magnitude of RC. Thus, searching for magnetic solids that exhibit promising magneto-caloric materials, especially the ones with a table-shaped performance, is one of the most important issues for MC. For this purpose, magnetic alloys and compounds have been fabricated or designed and systematically checked with their MCE performances.[7–10]

Moreover, researchers have focused on magneto-caloric performances in some selected heavy rare-earth (RE) rich magnetic alloys in amorphous states due to their promising applications.[11–13] Compared with the crystallized HRE-rich alloys or compounds, the magnetic-entropy-change maxima, i.e., $|\Delta S_M|$, for the alloys in amorphous states are usually smaller. However, magnetic transitions for the alloys in amorphous states are somehow broader, since there is no long-range ordering which will widen the peak of $|\Delta S_M(T)|$ curves. Previous investigations have demonstrated that most of the heavy rare-earth based alloys could be synthesized as amorphous formulae with a similar wide composition region.[14] Moreover, according to the de Gennes factor, i.e., $(g_J-1)^2J(J+1)$, the magnetic phase transition temperature decreases gradually with increasing atomic number from Gd to Tm, which means that Tm-based compounds should possess the lowest phase-transition temperature.[4,5] Therefore, the temperature range of the magnetic phase transition would be further widened by alloying different RE elements with proper ratios, which may induce a table-shaped MCE. On this purpose, the multiple heavy RE-based $Gd_{20}Ho_{20}Tm_{20}Cu_{20}Ni_{20}$ amorphous ribbons were selected and successfully fabricated, and the table-shaped MCE with large RC values were realized.

The $Gd_{20}Ho_{20}Tm_{20}Cu_{20}Ni_{20}$ alloy ingot was fabricated by arc-melting the bulk metals of Ho, Tm, Gd, Cu, and Ni (purity $\geq$ 99.9 wt.%) with Ti-getter under high-purity Ar-gas. The ingots were flipped and re-melted 4 times; and the

*Project supported by the National Natural Science Foundation of China (Grant No. 52071197), the Science and Technology Committee of Shanghai (Grant No. 19ZR1418300), and the Independent Research and Development Project of State Key Laboratory of Advanced Special Steel, Shanghai Key Laboratory of Advanced Ferrometallurgy, Shanghai University (Grant No. SKLASS 2019-Z003), and the Science and Technology Commission of Shanghai Municipality (Grant No. 19DZ2270200).

†Corresponding author. E-mail: ykzhang@shu.edu.cn

© 2021 Chinese Physical Society and IOP Publishing Ltd

weight loss was ~0.4 wt.% during this process. Then, the amorphous ribbons with width of 2.0–3.2 mm and thickness of 30–40 μm were obtained from the ingot by the melt-spun method under high-purity Ar-gas using Cu-wheel (33 m/s surface speed). The structures were checked by x-ray diffraction (XRD, Bruker-D8). The microstructure and elemental distribution was determined by a high resolution (HR) transmission electron microscope (TEM) with an attached energy-dispersive x-ray (EDX) diffractometer (JEOL JEM-2010). The magnetization data was collected using a commercial superconducting quantum interference device (SQUID, QD) and the ribbon is paralleled to the magnetic field to minimize the shape anisotropy effect.

Figure 1(a) illustrates the XRD pattern of $Gd_{20}Ho_{20}Tm_{20}Cu_{20}Ni_{20}$ spun ribbons. A broad diffraction halo in the angle range of 25°–40° is observed without obvious crystalline diffraction peaks, i.e., $Gd_{20}Ho_{20}Tm_{20}Cu_{20}Ni_{20}$ ribbons are with amorphous state and without crystalline phases. The microstructure of $Gd_{20}Ho_{20}Tm_{20}Cu_{20}Ni_{20}$ ribbons was examined by HRTEM, as shown in Fig. 1(b). The inset of Fig. 1(b) illustrates the selected area electron-diffraction (SAED) pattern for $Gd_{20}Ho_{20}Tm_{20}Cu_{20}Ni_{20}$ ribbons. The HRTEM image and SAED pattern can further confirm that the present $Gd_{20}Ho_{20}Tm_{20}Cu_{20}Ni_{20}$ ribbons are with full amorphous structures. The EDX mapping results for all the consistent elements (Gd, Ho, Tm, Cu, and Ni) are given in Figs. 1(c)–1(g), respectively, which clearly indicate that all the consistent elements are uniformly distributed in $Gd_{20}Ho_{20}Tm_{20}Cu_{20}Ni_{20}$ amorphous ribbons, and the atom percentages of Gd, Ho, Tm, Cu, and Ni are 19.92 at.%, 18.64 at.%, 17.85 at.%, 22.36 at.%, and 21.23 at.%, respectively.

Figure 2(a) illustrates the $M(T)$ curves for $Gd_{20}Ho_{20}Tm_{20}Cu_{20}Ni_{20}$ amorphous ribbons. One can note that no obvious differences in $M(T)$ curves for $H = 0.2$ T can be found between the zero-field-cooled curve and the field cooled ones. Moreover, the external fields have significant effects on the magnetic transition for $Gd_{20}Ho_{20}Tm_{20}Cu_{20}Ni_{20}$ amorphous ribbons, a pronounced sharp transition from paramagnetic (PM) to ferromagnetic (FM) state happens at Curie temperature T_C of 32 K under low H (0.2 T), and the transition is continuously becoming wider with increasing H. Especially, for the 5 and 7 T from 10 to 80 K, an almost linear relationship between the magnetization and temperature is observed, i.e., the magnetic transition is flat and continuous under high magnetic fields. Such a character could be easily identified in the dM/dT versus T data of the $Gd_{20}Ho_{20}Tm_{20}Cu_{20}Ni_{20}$ amorphous ribbons, as represented in Fig. 2(b). dM/dT has a significant change from a sharp to a flat and then to a table-like feature with increasing H.

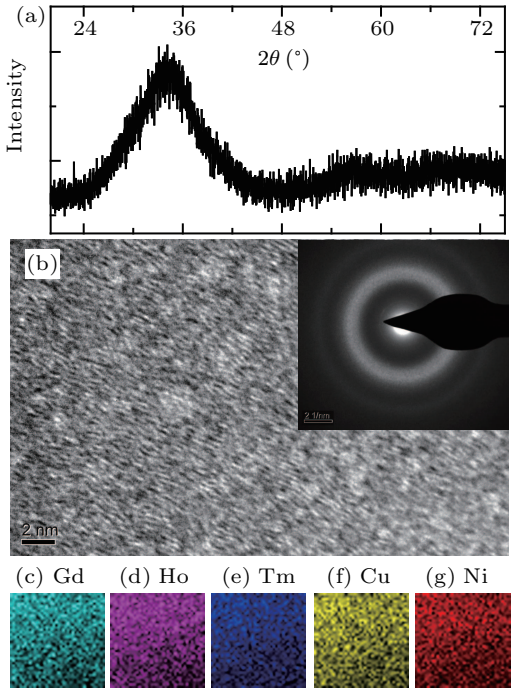


Fig. 1. (a) XRD pattern, (b) HRTEM images, and (c)–(g) EDX mapping for $Gd_{20}Ho_{20}Tm_{20}Cu_{20}Ni_{20}$ amorphous ribbons. Inset of (b) shows the SAED pattern for $Gd_{20}Ho_{20}Tm_{20}Cu_{20}Ni_{20}$ amorphous ribbons.

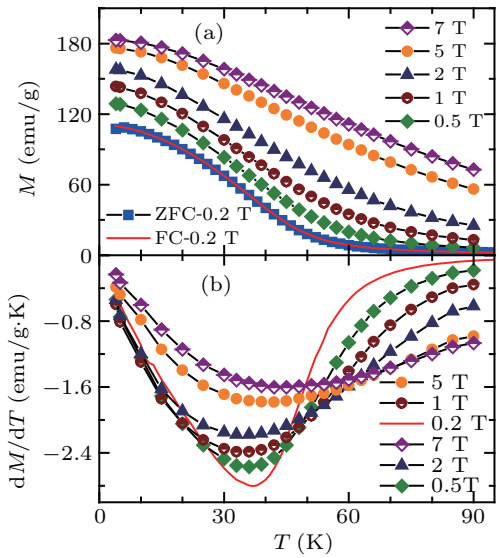


Fig. 2. (a) The $M(T)$ curves for $Gd_{20}Ho_{20}Tm_{20}Cu_{20}Ni_{20}$ amorphous ribbons with H up to 7 T. (b) The dM_{FC}/dT versus T for $Gd_{20}Ho_{20}Tm_{20}Cu_{20}Ni_{20}$ amorphous ribbons.

Several selected $M(H)$ curves for $Gd_{20}Ho_{20}Tm_{20}Cu_{20}Ni_{20}$ amorphous ribbons are illustrated in Fig. 3(a). At low H, M increases rapidly for lower temperature ones and demonstrates a saturation-like behavior with further increasing magnetic field, i.e., the $Gd_{20}Ho_{20}Tm_{20}Cu_{20}Ni_{20}$ ribbons exhibit a typical behavior as FM ordering amorphous materials. Furthermore, the magnetic phase transition for amorphous $Gd_{20}Ho_{20}Tm_{20}Cu_{20}Ni_{20}$ ribbons is detailedly analyzed by Arrott plots (M^2 versus H/M) and Banerjee criterion, as illustrated in Fig. 3(b).[16] No negative slope or inflection could be found as a character for the first-order magnetic transition,

suggesting that the phase transition in the present amorphous $Gd_{20}Ho_{20}Tm_{20}Cu_{20}Ni_{20}$ ribbons is of a second-order type.

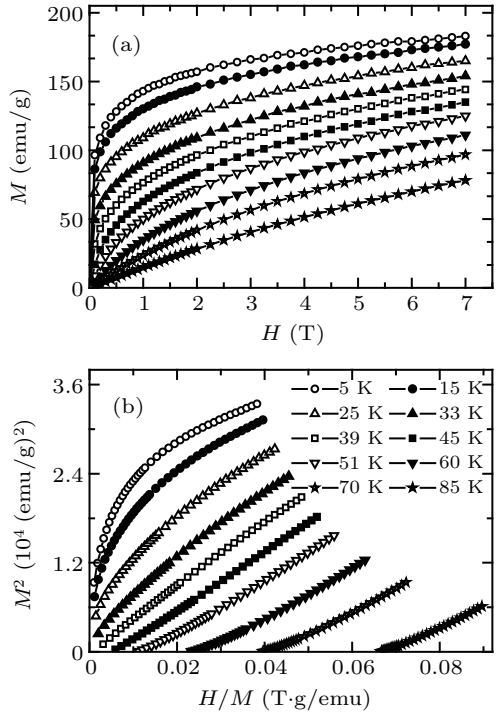


Fig. 3. (a) Selected $M(H)$ data for $Gd_{20}Ho_{20}Tm_{20}Cu_{20}Ni_{20}$ ribbons. (b) The corresponding plots of H/M vs M^2.

Generally, the ΔS_M with external field change of 0–H^{max} was evaluated by Maxwell's thermo-dynamic relation with integrating over the isothermal magnetization curves:[1–3]

$$\Delta S_M(T,\Delta H) = S_M(T,H) - S_M(T,H_0) = \int_0^H \left(\frac{\partial M(H,T)}{\partial H}\right)_T \mathrm{d}H. \quad (1)$$

Using Maxwell's relation

$$\left(\frac{\partial S}{\partial H}\right)_T = -\left(\frac{\partial M}{\partial T}\right)_H, \quad (2)$$

then

$$\Delta S_M(T,\Delta H) = \int_0^H \left(\frac{\partial M(H,T)}{\partial T}\right)_H \mathrm{d}H. \quad (3)$$

The temperature (T) dependence of $|\Delta S_M|$ for $Gd_{20}Ho_{20}Tm_{20}Cu_{20}Ni_{20}$ amorphous ribbons evaluated by Eq. (3) is illustrated in Fig. 4. Generally, all the $|\Delta S_M|(T)$ curves exhibit table shapes, which are very useful for Ericsson MC cycles. The peculiar MCE performance in $Gd_{20}Ho_{20}Tm_{20}Cu_{20}Ni_{20}$ amorphous ribbons is probably related to the unique characteristics of amorphous alloys, i.e., uniform consistent elements, especially for the multiple rare earth elements and the state of fully amorphous alloys. Additionally, the external magnetic field sensitive dependence of the magnetic transition is also considered to be one of an important factor on the table-shaped MCE behavior, which can be found in the previously reported crystallized Eu_4PdMg compound.[20] The deduced maxima $|\Delta S_M|$ ($|\Delta S_M|^{max}$) are 13.9, 10.6, 4.7, and 2.4 J/kg·K for ΔH = 0–7, 0–5, 0–2, and 0–1 T, respectively. While these values are smaller than those of $ErCo_2$ (38.0 J/kg·K for ΔH = 0–5 T) and $ErAl_2$ (36.15 J/kg·K for ΔH = 0–5 T),[23,24] the present $Gd_{20}Ho_{20}Tm_{20}Cu_{20}Ni_{20}$ amorphous ribbons can cover much wider temperature range which is beneficial for active applications. The $|\Delta S_M|^{max}$ values under low ΔH for $Gd_{20}Ho_{20}Tm_{20}Cu_{20}Ni_{20}$ amorphous ribbons are larger than most of the reported table-shaped MCE materials, such as $Gd_{50}Co_{45}Fe_5$ (~1.1 J/kg·K for 0–1 T, and ~2.0 J/kg·K for 0–2 T),[13] Eu_4PdMg (2.6 J/kg·K for 0–2 T),[15] and EuAuGe (3.5 J/kg·K for 0–2 T).[19]

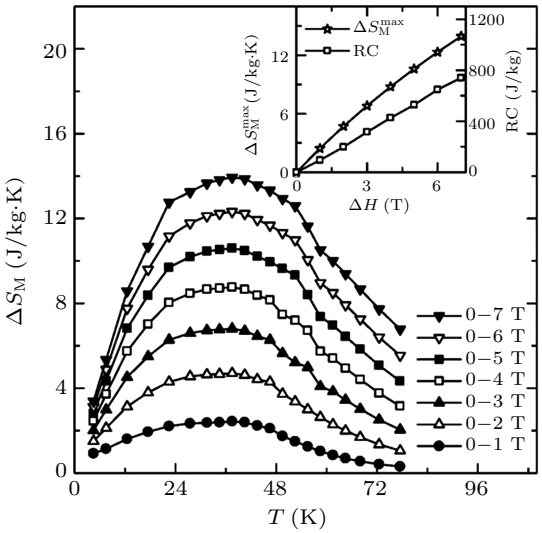


Fig. 4. $|\Delta S_M|(T)$ for $Gd_{20}Ho_{20}Tm_{20}Cu_{20}Ni_{20}$ amorphous ribbons. Inset: ΔH dependence of the $-\Delta S_M^{max}$ and RC.

Additionally, Griffith *et al.* have applied the temperature-averaged $g\Delta S_M$ (i.e., TEC) to characterize the magneto-caloric performances.[17] It is described that the MCE materials can reasonably response to the temperature lift (ΔT_{lift}), and it is defined as

$$\mathrm{TEC}(\Delta T_{lift}) = \frac{1}{\Delta T_{lift}} \max_{T_{mid}} \left\{ \int_{T_{mid}-\frac{T_{lift}}{2}}^{T_{mid}+\frac{\Delta T_{lift}}{2}} \Delta S(T)\,\mathrm{d}T \right\}, \quad (4)$$

where T_{mid} denotes the value of the average temperature. The TEC is calculated at 10 K temperature lift [TEC(10), and the values are 2.39, 4.67, 10.52, and 13.84 J/kg·K for ΔH = 0–1, 0–2, 0–5, and 0–7 T, respectively. Obviously, the $|\Delta S_M|^{max}$ and TEC(10) values are close to each other with the same ΔH, which is the consequence of the table-shaped MCE and the ΔT_{lift} value of 10 K is much lower than the full width at half maximum (δT_{FWHM}) in the ΔS_M–T curves for $Gd_{20}Ho_{20}Tm_{20}Cu_{20}Ni_{20}$ ribbons.

In addition, RC is another crucial parameter which can justify the MCE performances. Detailed description of the calculation method of RC is given in our review articles.[1] The

obtained values of $\delta T_{\rm FWHM}$ are 65.1 and 60.8 K for $\Delta H = 0$–7 and 0–5 T, respectively. Correspondingly, the RC values for the present $Gd_{20}Ho_{20}Tm_{20}Cu_{20}Ni_{20}$ amorphous ribbons are evaluated to be 528 and 740 J/kg. The transition temperature ($T_{\rm C}$), the $\delta T_{\rm FWHM}$, $|\Delta S_{\rm M}|^{\rm max}$ and RC values for $Gd_{20}Ho_{20}Tm_{20}Cu_{20}Ni_{20}$ amorphous ribbons and several reported promising magneto-caloric materials with close working temperature span under $\Delta H = 0$–5 T are listed in Table 1. Obviously, these $\delta_{\rm FWHM}$, $|\Delta S_{\rm M}|^{\rm max}$, and RC values for $Gd_{20}Ho_{20}Tm_{20}Cu_{20}Ni_{20}$ amorphous ribbons are quite competitive. In other words, the obtained promising MCE parameters for the present $Gd_{20}Ho_{20}Tm_{20}Cu_{20}Ni_{20}$ amorphous ribbons, especially for large values of $\delta_{\rm FWHM}$ and RC, together with the observed table-shaped MCE, make them considerable for cryogenic MC.

Table 1. The MCE parameters ($T_{\rm C}$, $g\delta T_{\rm FWHM}$, $-\Delta S_{\rm M}^{\rm max}$, RC) for $\Delta H = 0$–5 T for $Gd_{20}Ho_{20}Tm_{20}Cu_{20}Ni_{20}$ and several reported promising magneto-caloric solids with similar $T_{\rm C}$.

Materials	$T_{\rm C}$ (K)	$\delta T_{\rm FWHM}$ (K)	$\lvert\Delta S_{\rm M}\rvert^{\rm max}$ (J/kg·K)	RC (J/kg)	References
$Gd_{20}Ho_{20}Tm_{20}Cu_{20}Ni_{20}$	32	60.8	10.6	528	present
$ErZn_2$/ErZn	20	20	19.5	362	[6]
HoPdIn	23	34	14.6	432	[19]
$TbCoC_2$	30	35	15.3	367	[20]
Dy_2Cu_2Cd?/Tm_2Cu_2Cd	36	52	11	417	[21]
Ho_3Ni_2	30	33	19.4	371	[22]

In summary, high quality $Gd_{20}Ho_{20}Tm_{20}Cu_{20}Ni_{20}$ amorphous ribbons have been successfully fabricated by melt-spun technology, and the microstructure, magnetism, magnetic transition and magneto-caloric performances have been investigated. The $Gd_{20}Ho_{20}Tm_{20}Cu_{20}Ni_{20}$ ribbons are confirmed to reveal fully amorphous state without any crystallized phase and the consistent elements are all distributed uniformly. The $Gd_{20}Ho_{20}Tm_{20}Cu_{20}Ni_{20}$ amorphous ribbons demonstrate an external field sensitive magnetic transition, and exhibit a table-like shape magneto-caloric performance. With $\Delta H = 0$–5 T, the calculated $\Delta S_{\rm M}^{\rm max}$, $\delta T_{\rm FWHM}$, TEC(10) and RC values reach -10.6 J/kg·K, 60.8 K, -10.52 J/kg·K, and 528 J/kg, respectively. The promising MCE performances indicate that $Gd_{20}Ho_{20}Tm_{20}Cu_{20}Ni_{20}$ amorphous ribbons are also considerable candidate for MC.

Acknowledgement

The authors thank Analysis and Test Center of Shanghai University for providing the instrument.

References

[1] Franco V, Blázquaz J S, Ipus J J, Law J Y, Moreno-Ramíreza L M and Conde A 2018 *Prog. Mater. Sci.* **93** 112
[2] Zhang Y K 2019 *J. Alloys Compd.* **787** 1173
[3] Li L W and Yan M 2020 *J. Alloys Compd.* **823** 153810
[4] Shen B G, Sun J R, Hu F X, Zhang H W and Cheng Z H 2009 *Adv. Mater.* **21** 4545
[5] Smaïli A and Chahine R 1997 *J. Appl. Phys.* **81** 824
[6] Li L W, Yuan Y, Qi Y, Wang Q and Zhou S Q 2018 *Mater. Res. Lett.* **6** 67
[7] Zhang Y K, Guo D, Wu B B, Wang H F, Guan R G, Li X and Ren Z M 2020 *J. Alloys Compd.* **817** 152780
[8] Li L, Xu P, Ye S, Li Y, Liu G, Huo D and Yan M 2020 *Acta Mater.* **194** 354
[9] Wu B, Zhang Y, Guo D, Wang J and Ren Z 2020 *Cera. Int.* (in press)
[10] Zhang Y K, Li H D, Geng S H, Lu X G, Wilde G 2019 *J. Alloys Compd.* **770** 849
[11] Guo D, Zhang Y, Wang Y, Wang J and Ren Z 2020 *Chin. Phys. B* **29** 107502
[12] Li L W, Xu C, Yuan Y and Zhou S Q 2018 *Mater. Res. Lett.* **6** 413
[13] Wang Y, Guo D, Wu B, Geng S and Zhang Y 2020 *J. Magn. Magn. Mater.* **498** 166179
[14] Wang W H 2009 *Adv. Mater.* **21** 4524
[15] Li L, Niehaus O, Kersting M, P?ttgen R 2014 *Appl. Phys. Lett.* **104** 092416
[16] Banerjee B K 1964 *Phys. Lett.* **12** 16
[17] Griffith L D, Mudryk Y, Slaughter J, Pecharsky V K 2018 *J. Appl. Phys.* **123** 034902
[18] Zhang Y K, Wilde G 2016 *J. Supercond. Nov. Magn.* **29** 2159
[19] Li L W, Namiki T, Huo D X, Qian Z H, Nishimura K 2013 *Appl. Phys. Lett.* **103** 222405
[20] Li B, Hu W J, Liu X G, Yang F, Ren W J, Zhao X G, Zhang Z D 2008 *Appl. Phys. Lett.* **92** 242508
[21] Zhang Y K, Yang Y, Xu X, Geng S H, Hou L, Li X, Ren Z M and Wilde G 2016 *Sci. Rep.* **6** 34192
[22] Dong Q Y, Chen J, Shen J, Sun J R, Shen B G 2011 *Appl. Phys. Lett.* **99** 132504
[23] Zou J D, Shen B G and Sun J R 2007 *Chin. Phys.* **16** 1817
[24] Lima A L, Gschneidner Jr K A, Pecharsky V K and Pecharsky A O 2003 *Phys. Rev. B* **68** 134409